Research Paper

# Phase-transitional Fe₃O₄/perfluorohexane Microspheres for Magnetic Droplet Vaporization

Ronghui Wang[1]; Yang Zhou[1]; Ping Zhang[1]; Yu Chen[3]; Wei Gao[1]; Jinshun Xu[1]; Hangrong Chen[3]; Xiaojun Cai[3]; Kun Zhang[3]; Pan Li[1]; Zhigang Wang[1]; Bing Hu[2✉]; Tao Ying[2✉]; Yuanyi Zheng[1,2✉]

1. Second Affiliated Hospital of Chongqing Medical University, 76 Linjiang Road, Chongqing, 400016, P. R. China
2. Shanghai Institute of Ultrasound in Medicine, Shanghai Jiaotong University affiliated Sixth People's Hospital, Shanghai, 200233, P. R. China.
3. State Key Laboratory of High Performance Ceramics and Superfine microstructure, Shanghai Institute of Ceramics, Chinese Academy of Sciences, 1295 Dingxi Road, Shanghai, 200050, P. R. China

✉ Corresponding authors: yingtaomail@yeah.net, binghu_stephen@163.com, zhengyuanyi@gmail.com

## Abstract

Activating droplets vaporization has become an attractive strategy for ultrasound imaging and physical therapy due to the significant increase in ultrasound backscatter signals and its ability to physically damage the tumor cells. However, the current two types of transitional droplets named after their activation methods have their respective limitations. To circumvent the limitations of these activation methods, here we report the concept of magnetic droplet vaporization (MDV) for stimuli-responsive cancer theranostics by a magnetic-responsive phase-transitional agent. This magnetic-sensitive phase-transitional agent—perfluorohexane (PFH)-loaded porous magnetic microspheres (PFH-PMMs), with high magnetic-thermal energy-transfer capability, could quickly respond to external alternating current (AC) magnetic fields to produce thermal energy and trigger the vaporization of the liquid PFH. We systematically demonstrated MDV both in vitro and in vivo. This novel trigger method with deep penetration can penetrate the air-filled viscera and trigger the vaporization of the phase-transitional agent without the need of pre-focusing lesion. This unique MDV strategy is expected to substantially broaden the biomedical applications of nanotechnology and promote the clinical treatment of tumors that are not responsive to chemical therapies.

Key words: Magnetic droplet vaporization, Phase transition, Ultrasound imaging.

## Introduction

Recently, phase-transitional theranostic agents have become a hot topic in ultrasound molecular imaging and therapy research. Unlike conventional ultrasound microbubbles, they have better stability [1, 2] due to their liquid cores, which makes them more suitable for ultrasound imaging [3] and drug delivery [4, 5] at desired positions where they are activated to form microbubbles. More importantly, by exploding the cancer cells via the rapid and large increase in volume as droplets convert to gas bubbles [6, 7], the phase-transitional agents have pioneered a novel physical treatment strategy for cancer generating broad interests.

Currently, there are two types of developed phase-transitional agents named after their activation methods. Acoustic droplet vaporization (ADV) is activated by ultrasound [8, 9] and optical droplet vaporization (ODV) is triggered by laser [10]. These two activation methods have their limitations: ultrasound cannot penetrate the air-filled viscera and bone [11, 12] and laser activation is limited by tissue penetration depth [13]. More importantly, the activation region for both ADV and ODV must be determined before the application of ultrasound or laser hindering their further use in early tumor diagnosis and therapy when the location of the tumor

is unknown. Although ADV and ODV can address this challenge by scanning all organs to trigger the concentrated phase-transitional agents in tumor region, this solution is at the cost of extending the scanning time.

Magnetic hyperthermia employs alternating current (AC) magnetic field to generate thermal energy for tumor therapy. The electromagnetic wavelength can penetrate the air-filled viscera and bone, and its tissue penetration depth is deep enough for human body applications [14]. The range of magnetic field could cover the whole organs, and the energy could accurately deposit at the region where the phase transitional agents located. Given these merits, magnetic hyperthermia may serve as an ideal activation mechanism for droplet vaporization.

Herein, we developed a magnetic-responsive phase-transitional agent and tested its application and efficiency in droplet vaporization using the AC magnetic field. We named this strategy as "magnetic droplet vaporization (MDV)". As a prelude to the conceptual research, we validated the MDV at the level of intratumoral injection. Furthermore, we have explored the possibility of using these agents for magnetic hyperthermia therapy and intravascular administration.

## Materials and Methods

The animal experiments were approved by the Institutional Animal Care and Use Committee of Chongqing Medical University. The experimental design is illustrated in Figure 1.

### Mouse Tumor Model

Nude mice (Female; 4-6 weeks old; n=100) were acquired from Experimental Animal Center. The human MDA-MB-231 breast cancer cells suspension in the RPMI-1640 medium was subcutaneously injected into the right back of the nude mice (0.2 mL, $1 \times 10^6$ cells / mL per mouse). The mice with a tumor size of 0.8-1.2 cm were used for further experiments.

### Synthesis of PFH loaded Porous Magnetic Microspheres (PMMs)

Polymer microspheres of glycidyl methacrylate/ ethylene glycol dimethacrylate (GMA/ EGDMA) were synthesized using a modified method in the literature [15]. The P (GMA/EGDMA) microspheres were then treated with Ethylenediamine (EDA), $FeCl_3 \cdot 6H_2O$, $FeCl_2 \cdot 4H_2O$, ammonia hydroxide, and TEOS. After calcining at 600 °C, the porous magnetic microspheres (PMMs) with loose and porous inner structure were obtained. The PFH was imported inside the porous PMMs to obtain the PFH loaded PMMs (PFH-PMMs) using a negative pressure method. The detailed protocol for the synthesis is provided in the supplemental material.
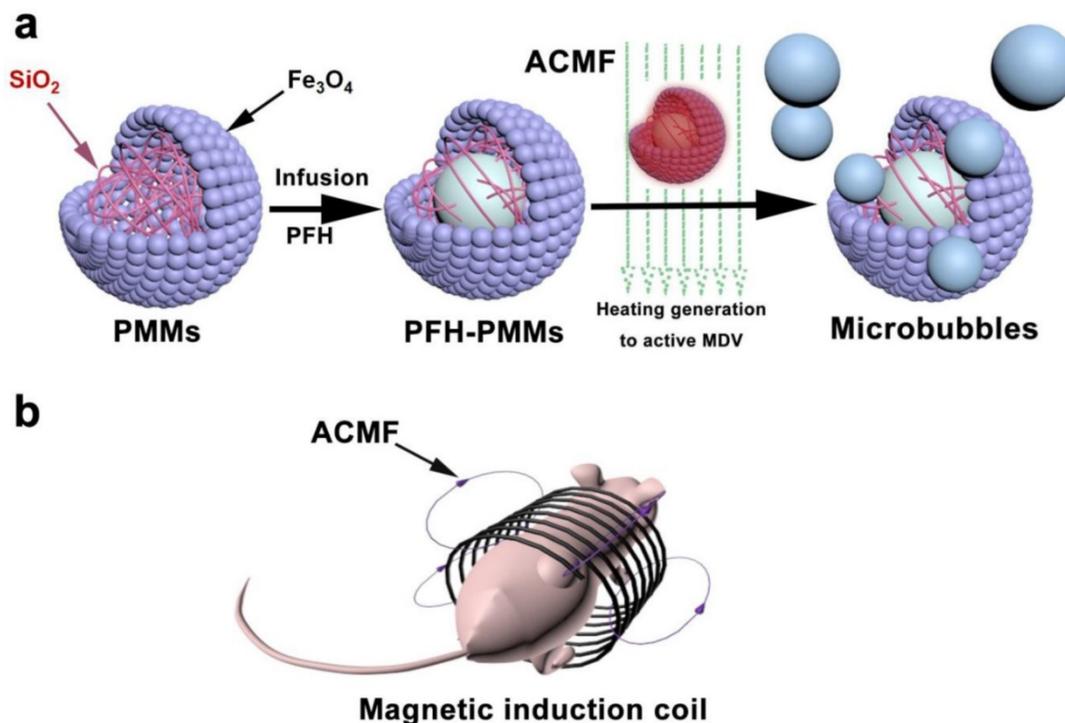


**Figure 1.** Schematics of tailored PFH encapsulation of PMMs for the novel MDV Stratery: a. Procedure for PFH-PMMs synthesis and the release of PFH-bubbles under an alternating current magnetic field (ACMF); b. PFH-PMMs in vivo subjected to heat treatment in nude mice.

## Characterizations

The following technologies were employed for the characterization of MDV: Scanning electron microscopy (SEM, S4800, Hitachi, Japan), transmission electron microscopy (TEM, HT7700, Hitachi, Japan), scanning transmission electron microscopy (STEM) and element mapping (Magellan 400, FEI company, Oregon, USA), Fourier Transform Infrared (FTIR) spectrum (Nicolet 7000-C, Thermal Nicolet Corporation, USA), Nitrogen adsorption-desorption isotherms (Micrometitics Tristar 3000 system, Norcross, USA), size distribution, zeta potential, stability testing (Nicomp TM 380 ZLS, PSS Nicomp particle size system, USA), and M-H curve (7410 Series VSM, Lake Shore Cryotronics, Westerville, USA).

## MDV Ability Evaluation

Ultrasound imaging: 1 mL of PFH-PMMs (10 mg mL$^{-1}$) and PMMs (10 mg mL$^{-1}$) were added to two bulbs of 3-mL pipettes. Subsequently, 8% polyvinyl alcohol (PVA) aqueous solution was added to these two bulbs (2 mL per bulb) to slow down the floating rate of the PFH-bubbles by enhancing the viscosity coefficient of the solvent. Ultrasonography (Transducer: LA523; Frequency: 4-13MHz; Depth: 3.7 cm; Derated Pressure: 105 kPa; Esoate: Mylab90, Italy) was used to observe the heating process of PFH-PMMs or PMMs in 70 °C water bath.

Evaluation of the Heat-producing Capacity: 0.5 mL of saline, PFH, and different concentrations (10 mg mL$^{-1}$, 20 mg mL$^{-1}$, and 40 mg mL$^{-1}$) of PFH-PMMs (6 samples per group) were separately exposed to AC magnetic field at 668 kHz fixed frequency, which was generated from a homemade magnetic hyperthermia machine for 270 seconds. The infrared thermal imaging (Ti32; Fluke, USA) was utilized to record magnetic heating process.

## MDV in Phantom

0.5 mL of Saline, PMMs (10mg mL$^{-1}$), and different concentrations of PFH-PMMs (10 mg mL$^{-1}$, 20 mg mL$^{-1}$, and 40 mg mL$^{-1}$) were dropped into the holes of the agarose gel phantom before and after AC magnetic field irradiation (6 samples per group). Ultrasound imaging (Transducer: LA523; Frequency: 4-13MHz; Depth: 3.7 cm; Derated Pressure: 105 kPa; Esoate: Mylab90, Italy) was utilized to capture the images.

## MDV in Mouse Tumor Model

The anesthetized tumor-bearing nude mice were randomly divided into three groups (6 mice per group) and were separately injected intratumorally with 0.2 mL of saline, PMMs (40 mg mL$^{-1}$), and PFH-PMMs (40 mg mL$^{-1}$). Ultrasonography (Transducer: LA523; Frequency: 4-13MHz; Depth: 2.2 cm; Derated Pressure: 110 kPa; Esoate: Mylab90, Italy) was used to capture the pre- and post-injection images of tumors. After imaging, these nude mice were placed in a magnetic induction coil (Diameter: 3 cm) for 6 min irradiation. Subsequently, the mice were scanned by ultrasonography.

## Magnetic Resonance Imaging in Mouse Tumor Model

12 tumor-bearing nude mice were divided into two groups (6 mice per group) and were injected with saline (0.1 mL) or PFH-PMMs (0.1 mL, 5 mg mL$^{-1}$). The mice were scanned pre- and post-injection by a 7.0 T Magnetic Resonance Imaging system (BioSpec 70/20USR, Bruker, Germany). The specific parameters of T2-weighted MR imaging were repetition time (TR) of 3000 ms, echo time (TE) of 45 ms, flip angle of 90°, matrix size of 256 × 256, section thickness of 0.3 mm and field of view (FOV) of 30 mm × 35 mm.

## Therapeutic Effect Evaluation

Tumor-bearing nude mice (n=48) were randomly separated into four groups (12 mice per group). The mice in different groups were injected with 0.2 mL of saline, PFH, PMMs (40mg mL$^{-1}$), and PFH-PMMs (40 mg mL$^{-1}$) and subsequently exposed to AC magnetic field at 668 kHz for 6 min a day for two days. The infrared thermal images and the temperature were acquired. After two treatments, half of the nude mice from the saline, PMMs, and PFH-PMMs groups were fed for 14 days to observe the variation of tumor volume. The second half of the nude mice were euthanized at 24 h after the second irradiation and their tumor tissues from the margin of the tumors were obtained for hematoxylin and eosin (H&E) stain, TUNEL, and Bcl-2 expression.

## Possibility of Application in Intravascular Administration

The nude mice (Female; 4-6 weeks old; n=6) from Experimental Animal Center received intravenous injections with 0.125 mL of 6 mg/mL PMMs-PFH into the tail vein. 3 h after injection, 6 of these nude mice were euthanized, and their liver tissue sections were obtained for Prussian blue stain.

## Statistical Analysis

Statistical analysis was performed with the SPSS software (version 22 for Mac; Chicago, USA). The values of particle size, zeta potential, and temperature were reported as mean ± standard deviation (SD). The gray scale values of ultrasound images in phantom that were not normal distribution were represented as

median (Interquartile range). The average diameter's difference of PFH-PMMs at different times was analyzed by Cruskal-Wallis test. Mann-Whitney U-test was used to compare the gray scale values' difference between pre- and post-AC magnetic field irradiation. The difference was considered significant when the P was less than 0.05.

## Results

Scanning electron microscopy (SEM) revealed that the PMMs obtained were of uniform size (Figure 2a). PMMs surface pores were confirmed by magnified SEM images, as shown in Figure 2b. The transmission electron microscope (TEM) revealed that the dark $Fe_3O_4$ particles were incorporated into PMMs shells. The discrepancy of contrast of scanning transmission electron microscope (STEM) images in the core indicated that the interior of the PMMs had a loose porous structure (Figure 2c-2d). The PMMs element distribution was further confirmed by element mapping (Figure 2e). The line scans result revealed that Fe was outside, Si was inside, and O was located throughout the PMMs validating that the outside and the inner shells of the particles were composed of $Fe_3O_4$ particles and Silica, respectively (Figure 2f). Fourier transform infrared (FTIR) spectra were used to confirm the chemical composition of PMMs. The vibration peaks at wavelengths of 1087 cm$^{-1}$ and 466 cm$^{-1}$ are the characteristic peaks of Si-O and Fe-O bonds, respectively [16, 17]. The GMA/EGDMA peaks had already faded away [18], implying that the template had been completely removed from the pores of the PMMs via calcination (Figure S1). $N_2$ adsorption-desorption isotherms of PMMs exhibited a typical IV type with Brunauer, Emmet and Teller (BET) surface areas of 58 m$^2$ g$^{-1}$ and Barrett, Joyner, and Halenda (BJH) pore volume of 0.41 cm$^3$ g$^{-1}$. The pore distribution indicated that the average pore size of PMMs was 22.7 nm (Figure S2). Dynamic light scattering (DLS) showed that the mean PMMs diameter was 845 ± 65.8 nm with a polydispersity index (PdI) of 0.279 ± 0.018 and a zeta potential of -23.9 ± 2.67 mV (Figure S3). The average diameter of the fabricated PFH-PMMs at 37 °C had no obvious change along with the time (P>0.05) (Figure S4). The M-H curve was obtained by a vibrating sample magnetometer (VSM) at room temperature (Figure S5). The PMMs curve showed that the microspheres with superparamagnetic property had a magnetization saturation value of 18.165 emu g$^{-1}$.

The process of vaporization recorded in real time by ultrasonography showed that bubbles were continuously released from PFH-PMMs at the bottom of the container and gradually rose to the surface of solution (Movie S1) while for the PMMs without PFH, few gas-bubbles were generated (Movie
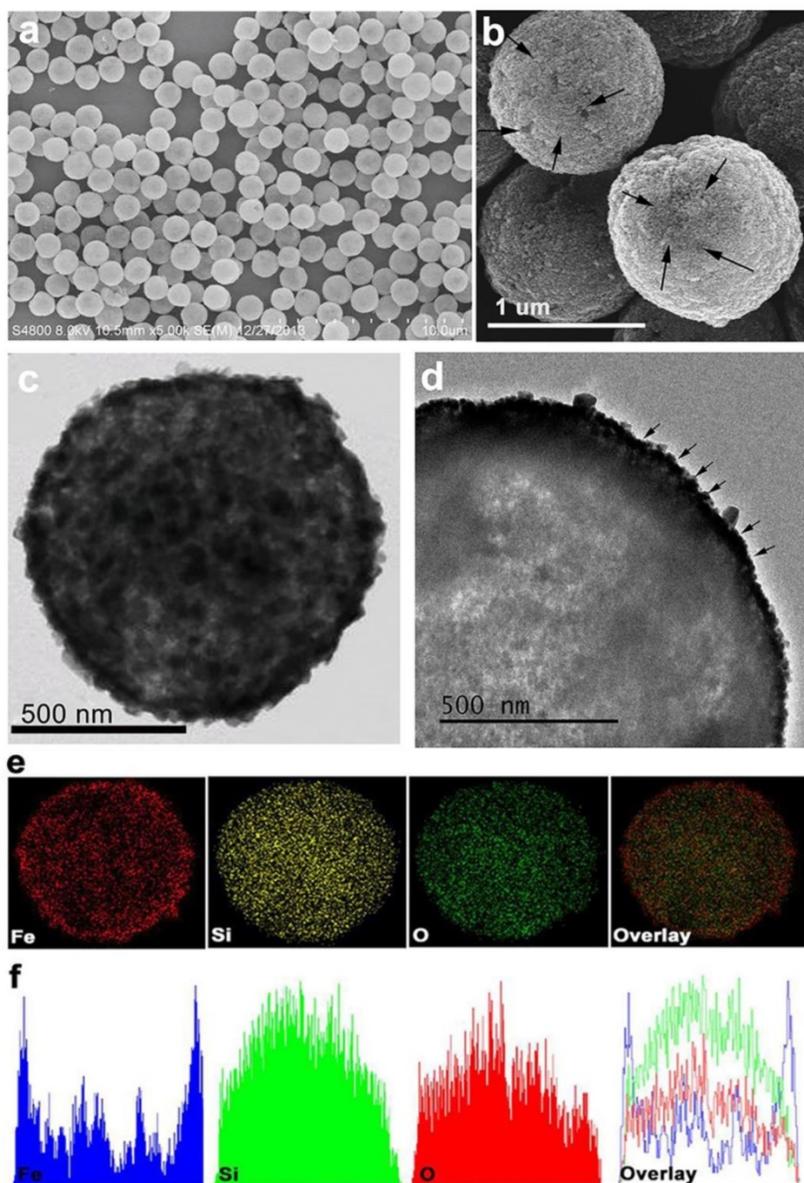


**Figure 2.** Characterization of PMMs by various imaging techniques: a-b. SEM images, c. STEM images, d. TEM images, e. element mapping f. element mapping corresponding line scans of PMMs corresponding line scans of PMMs.

S2). The infrared thermal images and the corresponding temperature-time curves clearly showed that the heat-producing capacity strongly depends on the concentration of PFH-PMMs (Figure 3a-3b). When microspheres were exposed to AC magnetic field, the temperature of PFH-PMMs (40 mg mL$^{-1}$) rose to >80˚C within 3 min (Figure 3a), whereas the temperatures of saline and PFH barely increased. Finally, optical microscopy was used to observe the 40 mg mL$^{-1}$ PFH-PMMs pre- and post- AC magnetic field treatment (Figure 3c-3d). The image showed that PFH-PMMs indeed generated bubbles under AC magnetic field (Figure 3d).

The echo intensity of saline, 10 mg mL$^{-1}$ PMMs, and different concentrations of PFH-PMMs pre- and post-magnetic heating treatment showed that the backscattering signal of ultrasound was indeed enhanced after PFH-PMMs were vaporized by electromagnetic energy, and the effect was strongly correlated with PFH-PMMs concentrations (Figure 4a). By analyzing the gray scale values obtained from B-mode and CEUS images, it was obvious that the gray scale values of PFH-PMMs at different concentrations were elevated after the magnetic field treatment ($P<0.05$). By contrast, the gray scale values of saline and 10 mg mL$^{-1}$ PMMs did not change noticeably (Figure 4b-4c).

The temperature distribution of nude mice captured by infrared thermal imaging confirmed that heat was only produced in the tumor region almost covering the entire tumor area when the mice injected with PMMs and PFH-PMMs were exposed to AC magnetic field for 180 s (Figure 5a). After 6 min of AC magnetic field exposure, the average temperatures of tumor region of mice from PMMs and PFH-PMMs groups increased to > 60 ˚C. By contrast, saline and PFH groups did not have an obvious temperature variation (Figure S6). Ultrasound images of tumor of nude mice from the PFH-PMMs group indicated that their ultrasonographic contrast was selectively enhanced after the irradiation of AC magnetic field (Figure 5b). The T$_2$-weighted images of tumors further illustrated the extensive ability of PFH-PMMs in negatively enhancing the contrast of magnetic resonance imaging (Figure S7).
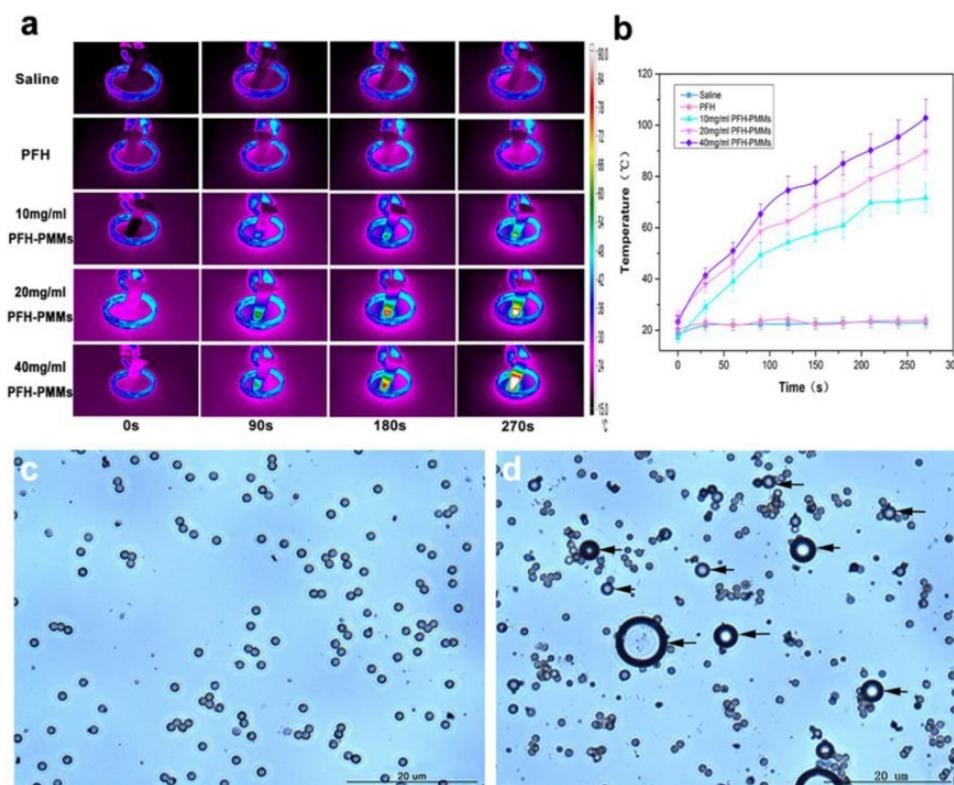


**Figure 3.** PFH-PMMs heating effect and MDV validation using optical microscopy: a. In vitro Infrared thermal images of heating in vitro; b. corresponding temperature-time curves; c-d. optical microscopy images of 40 mg mL$^{-1}$ PFH-PMMs pre- (c) and post- (d) AC magnetic field exposure for 3 min.
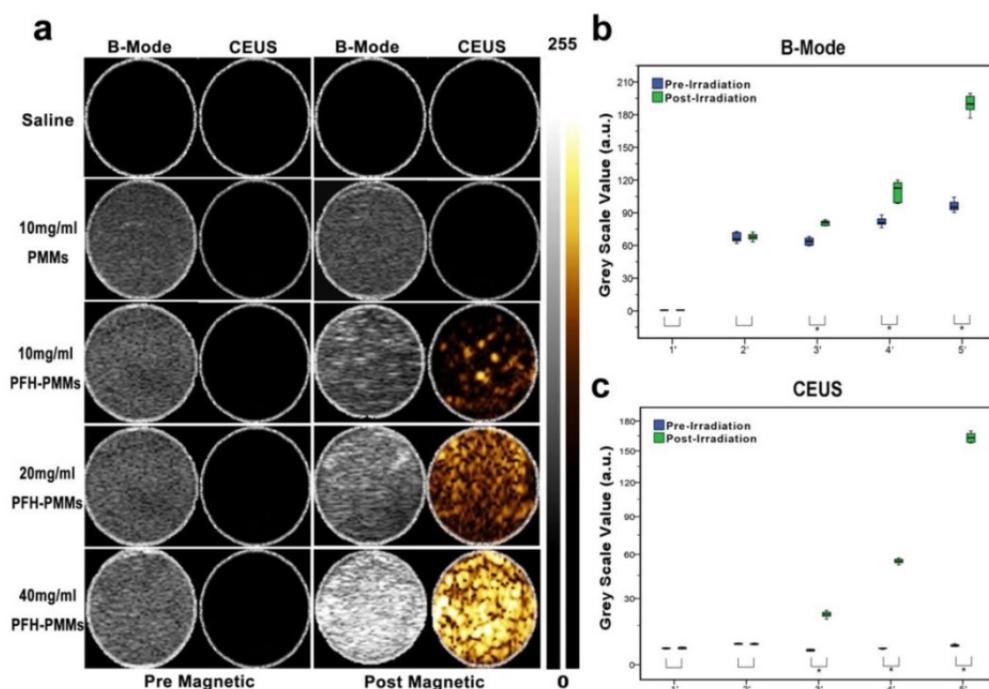
**Figure 4.** Evaluation of imaging performance: a. Ultrasound images of saline, 10 mg mL$^{-1}$ PMMs and different concentrations of PFH-PMMs in vitro; b-c. corresponding quantification of gray scale images in B-Mode and CEUS. * indicates significant differences (P≤0.05) based on gray scale values pre- and post-AC magnetic field irradiation (1'-5' separately represent saline, 10mg /mL PMMs, 10 mg/mL PFH-PMMs, 20 mg/mL PFH-PMMs, 40 mg/mL PFH-PMMs).
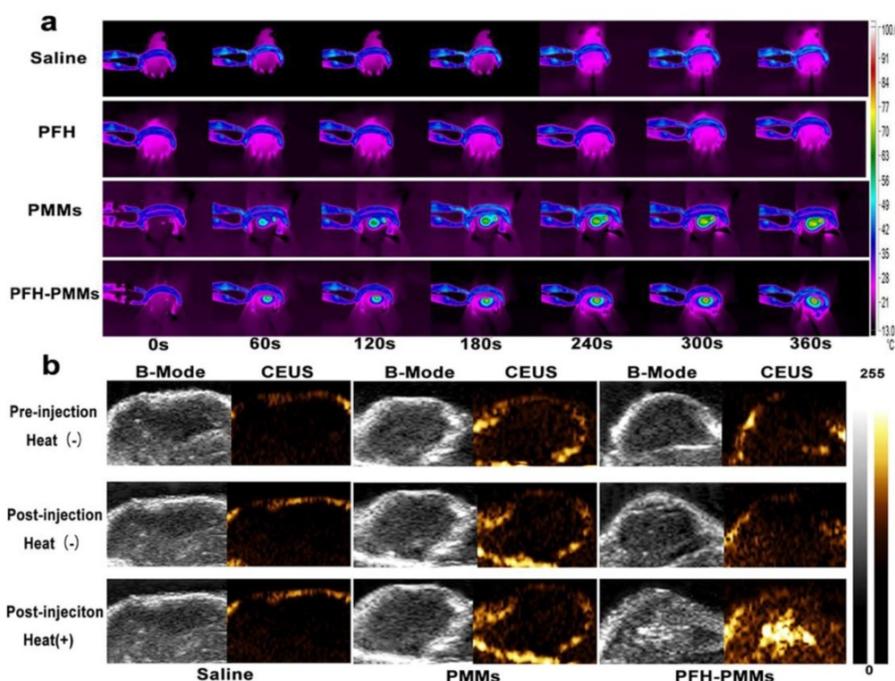


**Figure 5.** Infrared and ultrasound images in nude mice following various treatments: a. Infrared thermal images of thermotherapy temperatures in nude mice after intratumoral administration of saline, PFH, 40 mg mL$^{-1}$ PMMs or 40 mg mL$^{-1}$ PFH-PMMs; b. ultrasound images of tumors injected with saline, 40 mg mL$^{-1}$ PMMs or 40 mg mL$^{-1}$ PFH-PMMs pre- and post-magnetic heating treatment.

When subjected to magnetic heating twice, the tumor volumes of nude mice in PFH-PMMs and PMMs group were gradually decreased in the first two days, and the necrotic tumors fell off on the third day. The tumors of these nude mice were nearly eradicated without recurring in the 14 day-observation period. In comparison, the tumor volumes of nude mice in the saline group increased by nearly 3-fold (Figure 6a-6b). The tumor tissue slices from PFH-PMMs and PMMs groups showed a clear boundary between the central and peripheral tumor tissues, and the tumor cells in the central region
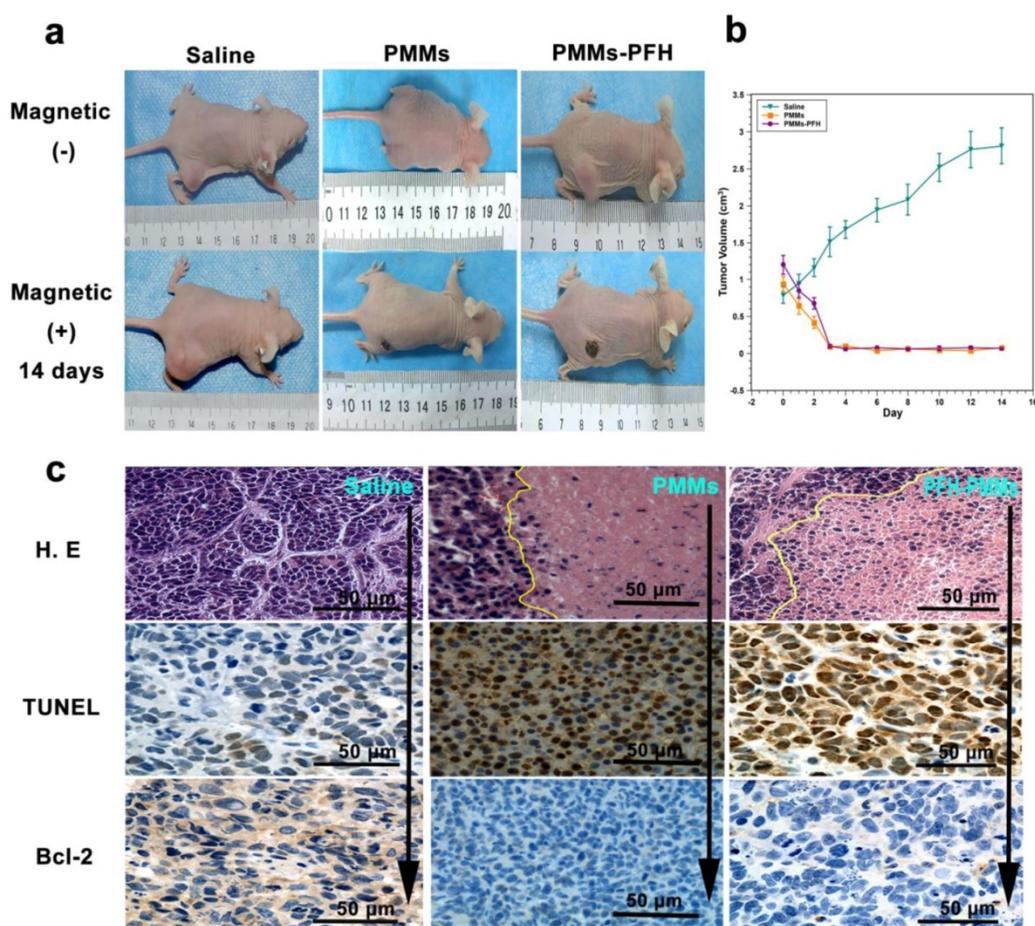
**Figure 6.** *In vivo* effects of PMMs and PFH-PMMS: a. Tumor (MDA-MB-231)-bearing nude mice treated with saline, PMMs and PFH-PMMs shown before and 14 days after a second magnetic heating treatment; b. Tumor growth curve of saline, PMMs and PFH-PMMs group after the exposure to the A.C. magnetic field. c. histopathological sections of tumor tissues from nude mice from the saline, PMMs and PFH-PMMs group.

showed coagulative necrosis. The immunohisto-chemical results of the PFH-PMMs group displayed TUNEL+ cells and low level of Bcl-2 expression in the cytoplasm of tumor cells. However, the saline group exposed to parallel AC magnetic field condition for 6 min showed nearly opposite staining results (Figure 6c). Simultaneously, liver tissue sections with Prussian Blue staining indicated that PMMs-PFH could reach remote tissues following intravascular administration (Figure S8).

## Discussion

In this study, we developed a magnetic responsive phase transitional agent, the PFH-PMMs, and confirmed its application and efficiency using the approach-MDV. Furthermore, we validated its use in hyperthermia therapy of tumors and potential applications in intravascular administration.

The MDV was accomplished by addressing two challenges: the magnetic agent's loading capacity and the response efficiency to AC magnetic field. For loading capacity, the tailored PMMs had a loose porous inner structure to encapsulate phase-transition liquid. The ability of loading PFH-droplets and releasing PFH-bubbles was strongly validated by the STEM images, quantitative analysis of data from $N_2$ adsorption-desorption isotherm, and the real-time observation of vaporization recorded by ultrasound imaging. For AC magnetic field responsive efficiency, $Fe_3O_4$ were coated on the surface of PMMs instead of being embedded in the shell to improve the efficiency in magnetic hyperthermia [19]. Furthermore, the loose porous silica inside the microspheres as the substitute for the template p(GMA/EGDMA) improved both biocompatibility [20] and thermal stability that guaranteed the continuous and steady release of PFH-bubbles during the heating process.

In addition to the challenges mentioned above, the selection of phase transitional liquid is also important for MDV. Temperature-sensitive PFH as phase transitional liquid is highly biocompatible and has a suitable boiling point (≈56˚C) [21]. Unlike the perfluoropentane (PFP) with a boiling point of 29 ˚C [22], the more stable PFH can avoid the irreversible vaporization during the fabricating process. Our stability test result also demonstrated that the

PFH-PMMs did not vaporize with time at normal temperature. Also, PFH-PMMs carried therapeutic as well as imaging functions. To achieve the therapeutic effect, the thermal ablation temperature produced by PFH-PMMs should be increased to >60˚C [13]. At this temperature, among the perfluorocarbons (PFCs), PFH may be the most appropriate choice as the phase transitional liquid for enhancing ultrasound imaging.

Infrared thermal imaging showed that the temperature raise was proportional to the concentration of PFH-PMMs, which could generate sufficient thermal energy to activate vaporization of PFH. Optical microscopy images directly confirmed the feasibility of MDV. Finally, ultrasound imaging was used to verify the ability of vaporized PFH-bubbles activated by AC magnetic field in enhancing ultrasonographic contrast in phantom.

Heating efficiency and MDV were validated *in vivo* by a series of animal experiments. By analyzing the infrared thermal images of nude mice captured in the course of magnetic heat treatment, we observed that the thermal energy produced by PFH-PMMs was sufficient to kill the tumor cells and shrink the tumor since the average temperatures in the tumor region could be increased to > 60 ˚C in 6 min. According to a previous report, the tumor cells undergo cell death under the high-temperature environment (>45˚C) [23]. Furthermore, the high temperature generated by PFH-PMMs under AC magnetic fields could be used to activate the vaporization of PFH. The vaporized PFH bubbles were observed by ultrasound inside the tumor where the PFH-PMMs located. This result not only verified the feasibility of MDV, but also demonstrated that the non-focused AC magnetic fields might specifically deposit the thermal energy at a precise location where the sensitive magnetic probe aggregated by either direct injection, targeting, or the EPR effect.

By ultrasound imaging, PFH-PMMs may fail to provide the accurate location of lesions near the air-filled visceral or bone tissues. However, the ability of PFH-PMMS in enhancing MR imaging could overcome the intrinsic deficiency of ultrasound. The results of $T_2$-weighted images of tumors illustrated that PFH-PMMs could effectively improve the contrast of the MR imaging. These results demonstrated that the elaborately designed PFH-PMMs could act as a dual mode agent for US/MRI imaging to compensate their respective drawbacks, improve the sensitivity of molecular imaging, and ensure safety during the magnetic heating process. The combination of the US/MRI imaging modalities has the potential to precisely detect the tumor and to monitor the therapeutic process. Furthermore, the phase transitional perfluorocarbon which was encapsulated inside the magnetic particles is also used for ODV and ADV. Thus, PFH-PMMS could also be triggered by ultrasound and laser for concurrent MDV, ODV, and ADV.

Therapeutic effect of magnetic hyperthermia was further evaluated by monitoring tumor volume and histology. The tumors in nude mice in the PFH-PMMs and PMMs groups were almost eradicated without recurrence. The histopathology results of tumor tissue slices from PFH-PMMs and PMMs groups indicated that central tumor cells experienced protein denaturation and coagulative necrosis leading to irreversible damage to the tumor cells. Peripheral tumor cells also lost the malignancy due to the programmed cell death. However, the nude mice in the saline group exposed to the parallel AC magnetic field for 6 min did not show damage to the tumor cells. These tumor volume evaluations and histopathology results provided clear evidence that PFH-PMMs and PMMs could effectively eradicate tumors via selective heating during MDV and the core component responsible for the therapeutic effect of PMMs-PFH was the PMMs.

Our current study, as a preface to the conceptual research, only demonstrated the application of MDV at the level of intratumoral injection. However, the results of liver tissues stained with Prussian Blue indicated that PFH-PMMs could reach other organs through circulation. To attain the stability of PFH-PMMS in circulation and specific targeting to the tumor site, we plan to adopt the following established strategies: a) coating PFH-PMMs with polyethyleneglycol (PEG) or depleting host Kupffer cells using preinjection of clodronate liposomes to escape the macrophage uptake for improving the delivery efficiency and b) modifying the PFH-PMMs with ligands or antibodies for their targeted delivery in the tumor region. It is also of note that heat treatment of tumors by MDV has the same limitations as other hyperthermia methods, such as incomplete destruction of tumors followed by recurrence [13]. Therefore, we plan to combine thermotherapy with the chemotherapeutic drugs which might enhance the death of tumor cells in the peripheral and transitional regions. Thus, we will extend our future investigation to encapsulate drugs inside the PFH-PMMs for preventing tumor recurrence caused by incomplete destruction.

In summary, we have designed a novel trigger vaporization approach, MDV, and successfully demonstrated the use of this technique at the level of intratumoral administration. Also, the thermal energy generated by the magnetic agents can also be exploited to heat the tumor. Therefore, MDV, as a

novel concept, might have a wider range of applications in early diagnosis and treatment of tumors.

## Supplementary Material

Additional File 1:
Supplementary Figures.
http://www.thno.org/v07p0846s1.pdf
Additional File 2:
Movie S1. http://www.thno.org/v07p0846s2.mp4
Additional File 3:
Movie S2. http://www.thno.org/v07p0846s3.mp4

## Acknowledgements

## Competing Interests

The authors have declared that no competing interest exists.

## References

1. Lanza GM, Wickline SA. Targeted ultrasonic contrast agents for molecular imaging and therapy. Prog Cardiovasc Dis. 2001; 44(1): 13-31.
2. Wilson K, Homan K, Emelianov S. Biomedical photoacoustics beyond thermal expansion using triggered nanodroplet vaporization for contrast-enhanced imaging. Nat Commun. 2012; 3: 618.
3. Rapoport N, Gao Z, Kennedy A. Multifunctional nanoparticles for combining ultrasonic tumor imaging and targeted chemotherapy. J Natl Cancer Inst. 2007; 99(14): 1095-106.
4. Rapoport NY, Kennedy AM, Shea JE, et al. Controlled and targeted tumor chemotherapy by ultrasound-activated nanoemulsions/microbubbles. J Control Release. 2009; 138(3): 268-76.
5. Rapoport N. Phase-shift, stimuli-responsive perfluorocarbon nanodroplets for drug delivery to cancer. Wiley Interdiscip Rev Nanobiotechnol. 2012; 4(5): 492-510.
6. Wang CH, Kang ST, Lee YH, et al. Aptamer-conjugated and drug-loaded acoustic droplets for ultrasound theranosis. Biomaterials. 2012; 33(6): 1939-47.
7. Sun Y, Wang Y, Niu C, et al. Laser-Activatible PLGA Microparticles for Image-Guided Cancer Therapy In Vivo. Adv Funct Mater. 2014; 24: 7674-80.
8. Li DS, Kripfgans OD, Fabiilli ML, et al. Initial nucleation site formation due to acoustic droplet vaporization. Appl Phys Lett. 2014; 104(6): 063703.
9. Li DS, Kripfgans OD, Fabiilli ML, et al. Formation of toroidal bubbles from acoustic droplet vaporization. Appl Phys Lett. 2014; 104(6): 063706.
10. Strohm EM, Rui M, Kolios MC, et al. Optical droplet vaporization (ODV): photoacoustic characterization of perfluorocarbon droplets. IEEE International Ultrasonics Symposium. 2010: 495-8.
11. Kennedy JE. High-intensity focused ultrasound in the treatment of solid tumours. Nat Rev Cancer. 2005; 5(4): 321-7.
12. ter Haar G. Therapeutic applications of ultrasound. Prog Biophys Mol Biol. 2007; 93(1-3): 111-29.
13. Chu KF, Dupuy DE. Thermal ablation of tumours: biological mechanisms and advances in therapy. Nat Rev Cancer. 2014; 14(3): 199-208.
14. Derfus AM, von Maltzahn G, Harris TJ, et al. Remotely triggered release from magnetic nanoparticles. Adv Mater. 2007; 19: 3932-6.
15. He J, Yang C, Xiong X, et al. Preparation and characterization of monodisperse porous silica microspheres with controllable morphology and structure. J Polym Sci Part A Polym. Chem. 2012; 50: 2889-97.
16. Sakizci M, Alver BE, Alver Ö, et al. Spectroscopic and thermal studies of bentonites from Ünye, Turkey. J Mol Struct. 2010; 969: 187-91.
17. Chen Y, Jiang L, Wang R, et al. Injectable Smart Phase-Transformation Implants for Highly Efficient In Vivo Magnetic-Hyperthermia Regression of Tumors. Adv Mater. 2014; 26: 7468-73.
18. Krajnc P, Leber N, Štefanec D, et al. Preparation and characterisation of poly (high internal phase emulsion) methacrylate monoliths and their application as separation media. J Chromatogr A. 2005; 1065(1): 69-73.
19. Fang K, Song L, Gu Z, et al. Magnetic field activated drug release system based on magnetic PLGA microspheres for chemo-thermal therapy. Colloids and Surf B Biointerfaces. 2015; 136: 712-20.
20. Wang Y, He J, Chen J, et al. Synthesis of monodisperse, hierarchically mesoporous, silica microspheres embedded with magnetic nanoparticles. ACS Appl Mater Interfaces. 2012; 4(5): 2735-42.
21. Zhou Y, Wang Z, Chen Y, et al. Microbubbles from Gas-Generating Perfluorohexane Nanoemulsions for Targeted Temperature-Sensitive Ultrasonography and Synergistic HIFU Ablation of Tumors. Adv Mater. 2013; 25: 4123-30.
22. Fang JY, Hung CF, Liao MH, et al. A study of the formulation design of acoustically active liposphere as carriers for drug delivery. Eur J Pharm Biopharm. 2007; 67(1): 67-75.
23. Thakor AS, Gambhir SS. Nanooncology: the future of cancer diagnosis and therapy. CA Cancer J Clin. 2013; 63(6): 395-418.